Blowing Off Steam: Tuffisite Formation As a Regulator for Lava Dome Eruptions

Jackie E. Kendrick[1]*, Yan Lavallée[1], Nick R. Varley[2], Fabian B. Wadsworth[3], Oliver D. Lamb[1] and Jérémie Vasseur[3]

[1] Department of Earth, Ocean and Ecological Sciences, University of Liverpool, Liverpool, UK, [2] Facultad de Ciencias, Universidad de Colima, Colima, Mexico, [3] Department of Earth and Environmental Science, Ludwig-Maximilians-Universität, Munich, Germany

Tuffisites are veins of variably sintered, pyroclastic particles that form in conduits and lava domes as a result of localized fragmentation events during gas-and-ash explosions. Those observed *in-situ* on the active 2012 lava dome of Volcán de Colima range from voids with intra-clasts showing little movement and interpreted to be failure-nuclei, to sub-parallel lenses of sintered granular aggregate interpreted as fragmentation horizons, through to infilled fractures with evidence of viscous remobilization. All tuffisites show evidence of sintering. Further examination of the complex fracture-and-channel patterns reveals viscous backfill by surrounding magma, suggesting that lava fragmentation was followed by stress relaxation and continued viscous deformation as the tuffisites formed. The natural tuffisites are more permeable than the host andesite, and have a wide range of porosity and permeability compared to a narrower window for the host rock, and gaging from their significant distribution across the dome, we posit that the tuffisite veins may act as important outgassing pathways. To investigate tuffisite formation we crushed and sieved andesite from the lava dome and sintered it at magmatic temperatures for different times. We then assessed the healing and sealing ability by measuring porosity and permeability, showing that sintering reduces both over time. During sintering the porosity-permeability reduction occurs due to the formation of viscous necks between adjacent grains, a process described by the neck-formation model of Frenkel (1945). This process leads the granular starting material to a porosity-permeability regime anticipated for effusive lavas, and which describes the natural host lava as well as the most impervious of natural tuffisites. This suggests that tuffisite formation at Volcán de Colima constructed a permeable network that enabled gas to bleed passively from the magma. We postulate that this progressively reduced the lava dome's ability to seal and build pressure that drives explosions. Indeed, the time interval between explosions during 2007–2011 gradually increased before the onset of a period of quiescence starting in June 2011. We suggest that the permeability evolution during tuffisite formation has important consequences for modeling of gas-and-ash explosions, common at dome-forming volcanoes.

Keywords: lava dome, permeability, glass transition, sintering, tuffisite, outgassing, magma fragmentation, explosive activity

INTRODUCTION

One of the most remarkable demonstrations of volcanic conduit instability takes place at active lava domes, which regularly exhibit shifts in eruption style (Sparks, 1997). At one end of the spectrum lava domes result from the effusion of lavas whose internal permeability allows volatile outgassing. At the other end of the spectrum, occasional catastrophic explosive eruptions may disrupt lava domes if volatile pressure is able to build up (Cashman and Scheu, 2015). But within this range of activity, lava domes commonly display hourly to daily, small to intermediate gas-and-ash explosions with plume heights of hundreds of meters to several kilometers (e.g., Volcán de Colima, Mexico; Sakurajima, Japan; Santa Maria, Guatemala; Karymsky, Russia).
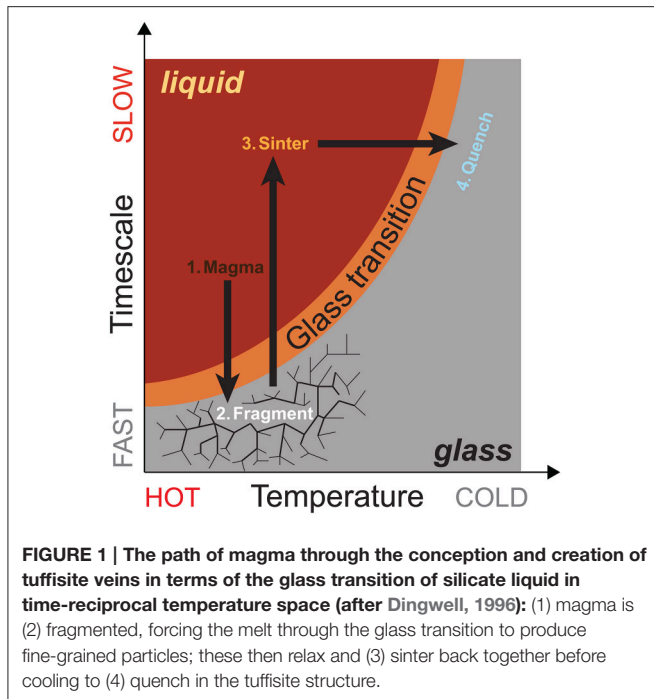
These explosions are generally thought to be the result of rapid decompression-driven, pore overpressurization that leads to magma fragmentation (Zhang, 1999; Gonnermann and Manga, 2003). Decompression not only leads to volatile exsolution from the melt as well as gas expansion, but also promotes crystallization (Cashman and Blundy, 2000), a process which releases latent heat (Blundy et al., 2006). Recent developments have seen a quantification of the influence of temperature fluctuations on the volatile budget of magma; whereby magma may be forced to rapidly vesiculate (degas) and fragment as a result of small temperature increments (Lavallée et al., 2015). Hence, it may be viewed that fragmentation increases degassing efficiency in silicic systems (Watts et al., 2002; Castro et al., 2014; Lavallée et al., 2015), and furthermore, relic fragmentation structures have been proposed as pathways that also allow passive bleeding of gases (Gonnermann and Manga, 2003; Castro et al., 2012; Burgisser and Degruyter, 2015) that may lower the explosive potential of an ongoing eruption. In addition, fragmentation has been linked to characteristic seismicity which occurs at shallow depth during magma migration (Neuberg, 2000; Green and Neuberg, 2006; Neuberg et al., 2006; Sahetapy-Engel et al., 2008; Palo et al., 2009; Varley et al., 2010; Arámbula-Mendoza et al., 2011; Thomas and Neuberg, 2012; Chouet and Matoza, 2013; Lamb et al., 2014; Webb et al., 2014; Arciniega−Ceballos et al., 2015). This seismicity can inform us of the timing of fragmentation events (e.g., Chouet, 1996), but when used in combination with field observations, can also provide information regarding subsurface processes and mechanisms that lead to fragmentation (e.g., Neuberg et al., 2006; Kendrick et al., 2014). For example, these explosions leave markers in the form of tuffisite veins; and understanding their formation can help us interpret the effects these small to moderate explosions have on the state of magma in conduits and lava domes.

Magma Fragmentation and Tuffisite Formation

Tuffisites are veins of variably sintered, indurated, fine grained pyroclastic material deposited in cracks and voids in lavas (Cloos, 1941; Stasiuk et al., 1996; Gonnermann and Manga, 2003; Tuffen et al., 2003; Noguchi et al., 2008; Castro et al., 2012; Kolzenburg et al., 2012; Berlo et al., 2013). The infiltration of fracture networks by hot gas and ash mixtures (Cloos, 1941; Tuffen et al.,

2003; Castro et al., 2012, 2014; Kolzenburg et al., 2012; Schipper et al., 2013) occurs during explosive volcanism as a result of subsurface fragmentation events. Tuffisites can both create or use pre-existing fractures (Stasiuk et al., 1996; Kolzenburg et al., 2012), and some tuffisites may represent the origin point of fragmentation events in the lava. Tuffisite veins show varying degrees of sintering or healing of the pyroclastic fragments (Stasiuk et al., 1996; Tuffen et al., 2003) and have also been shown to preserve massive to flow-banded or even bedded structures that form during turbulent, fluidized flow of the particulate material in the fractures (Tuffen et al., 2003). Typically, evidence for deformation of the surrounding host magma is minimal since tuffisites likely form during short-lived explosions that rip apart the hot magma (Kolzenburg et al., 2012; Castro et al., 2014).

So how is it that hot, "flowing" magma is able to fragment? Silicate melts can be viscoelastic fluids, which exhibit the glass transition (a rheological divide between the liquid and solid state). The glass transition can be cast in terms of temperature, timescale of relaxation, and melt chemistry (Webb and Dingwell, 1990). Melt behavior is only Newtonian at high temperatures or low local strain rates or low applied stresses. If temperature decreases or the deformation rate increases due to increased shear stresses (e.g., Papale, 1999) the magma becomes non-Newtonian. A typical mechanism by which deformation rates locally reach the values required for non-Newtonian behavior is when bubbles expand under especially large overpressures (e.g., Sahagian, 1999). If the deformation timescale further decreases (deformation rate increases) and approaches the timescale of local structural relaxation of the melt (i.e., the glass transition) then fracturing can occur as the melt exhibits increasingly elastic properties (e.g., Zhang, 1999). In this scenario, stress is no longer fully relaxed and instead is stored elastically until it overcomes the strength of the material, resulting in failure (Dingwell, 1996). This is thought to be the case in the creation of tuffisite veins during fragmentation that results from the build-up of pressurized gas phases (Alidibirov and Dingwell, 1996); pressurization eventually leads to hydrofracture (Voight et al., 1999) and propagation of a decompression wave (e.g., Fowler et al., 2010), a process that releases the gas and depressurizes the system. It is by behaving as a solid for short timescales that the melt is able to fail or fragment, and the once-coherent liquid can exist as fragments that are able to be transported through fractures. From the point at which failure relieves the bulk of the stress, the fractured material may relax any remaining stress viscously (e.g., Gonnermann, 2015), provided that temperature remains above the glass transition temperature (T_g). In the case of tuffisites, pyroclastic fragments that are trapped in fractures in the lava dome, in the magma column or in the country rock relax, reverting to a viscous mechanism and slowly sintering together, eventually healing the system (Tuffen et al., 2003). This provides a conceptual framework for how fracture-healing cycles occur in magmas (**Figure 1**); breaking into fragmental particles and healing back together in repetitive cycles of stress increase, followed by stress dissipation and sintering, which, after cooling provides a relic in the form of tuffisite. Although the sintering process has previously been explored theoretically (e.g., Mackenzie and Shuttleworth, 1949; Prado et al., 2001; Rahaman,

FIGURE 1 | The path of magma through the conception and creation of tuffisite veins in terms of the glass transition of silicate liquid in time-reciprocal temperature space (after Dingwell, 1996): (1) magma is (2) fragmented, forcing the melt through the glass transition to produce fine-grained particles; these then relax and (3) sinter back together before cooling to (4) quench in the tuffisite structure.

FIGURE 2 | Aerial view of Volcán de Colima with seismic station EZV4 location relative to the active vent at the lava dome. Insert 1: A small gas-and-ash explosion on 18 April 2009 at Volcán de Colima. Gas can be seen emerging from much of the dome surface. Insert 2: Map showing Volcán de Colima location in Mexico [Main image from Google Earth Pro V7.1.2.2041 (28/02/2015). Location: Volcán de Colima, Tonila, Mexico 19°30′50.40″N 103°37′12.00″W, Eye alt. 47,500 feet. DigitalGlobe 2016. http://earth.google.com (accessed October 14 2015)].

2008; Vasseur et al., 2013; Wadsworth et al., 2014), it is yet to encompass the complexity of natural crystal-bearing magmas. Likewise, while such cycles lead to ample preservation of tuffisites in glassy deposits at the surface (e.g., Stasiuk et al., 1996; Tuffen and Dingwell, 2005; Castro et al., 2014) they are rarely recognized in crystal-bearing magmas (Kolzenburg et al., 2012). Here, we explore the tuffisite formation process in crystalline magmas further, using Volcán de Colima (Mexico) as a case study.

Historic Activity at Volcán De Colima

Volcán de Colima is an active stratovolcano which, along with the extinct Nevado de Colima, forms the Colima Volcanic Complex, part of the Trans-Mexican Volcanic Belt (**Figure 2**). Over the last 400 years, the volcano has experienced ∼100 year cycles of effusive to explosive events. Throughout this period the lavas have been consistently andesitic (Luhr and Carmichael, 1980; Mora et al., 2002) with minor mafic excursions (relating to fresh mafic magma influx) that seem to dictate the cycle-ending (sub-)Plinian eruptions, the last one occurring in 1913 (Luhr, 2002). The crystal assemblage is predominantly plagioclase, with lesser amounts of orthopyroxene, clinopyroxene, and iron-titanium oxides set in interstitial glass (Luhr and Carmichael, 1980). Hornblende was present in the 1913 magmas, but not in subsequent eruptions, and olivine exists as xenocrysts. The lavas generally contain ∼30 vol.% phenocrysts, 25–50 vol.% microlites and 14–45 vol.% "dry" rhyolitic glass (Reubi and Blundy, 2008; Savov et al., 2008; Lavallée et al., 2012; Kendrick et al., 2013) with a bimodal porosity distribution peaking at 12 and 26% (Lavallée et al., 2012). Geothermometry of pyroxenes suggests relatively deep magma storage at temperatures of 960–1020°C (Savov et al., 2008), while melt inclusions verify this, indicating trapping conditions of 10–150 MPa and 959–1015°C (Reubi et al., 2013).
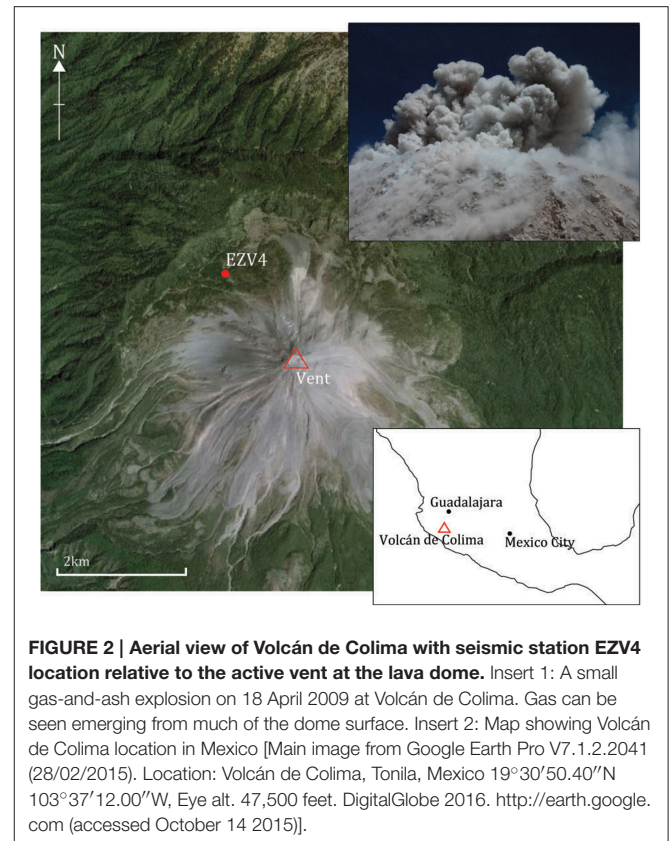
The andesite is largely degassed when it extrudes at the surface, and conduit temperature is estimated to exceed 940°C (Lavallée et al., 2012; Reubi et al., 2013). Outgassing has been shown to concentrate at the vent, with some geochemical indicators of impending activity recorded at summit fumaroles (Varley and Taran, 2003). Little diffuse outgassing has been recorded on the flanks, and the absence of a developed hydrothermal system has led to the inference of an impervious layer above the magma chamber (Varley and Taran, 2003). Recently, the eruptive period from November 1998 to June 2011 was characterized by episodic dome growth, lava flows and explosive events that waxed and waned (Zobin et al., 2002; Savov et al., 2008; Varley et al., 2010; Arámbula-Mendoza et al., 2011; Lavallée et al., 2012; Lamb et al., 2014). During this period, large Vulcanian events (column height > 5 km) occurred sporadically, with associated column collapses and pyroclastic flows (Gavilanes-Ruiz et al., 2009).

MATERIALS AND METHODS

The violent nature of magmatic fragmentation typically prevents us from accessing structures exposed in active lava domes, some of which may be formed during explosive eruptions; however, an 18-month period of quiescence at Volcán de Colima (Mexico) provided us with safe access (on 20th March 2012) to proximal fragmentation structures developed within the lava dome, protracted between 2007 and 2011. Here, we combine a field survey, monitored data,

experiments and modeling to gain insight into lava dome dynamics.

Monitoring

We explore the dome growth rate in the 4 years preceding the onset of quiescence on 21st June 2011. We compare this to explosion signals, manually classified and counted by *Colima Intercambio e Investigación en Vulcanología* (CIIV), recorded at a short-period instrument (EZV4), located ∼1.5 km from the vent (**Figure 2**). We then delve further into daily explosion rates in the year leading up to the halt in activity and question the link between geophysical data, geological observations and an understanding of the magmatic processes that lead to changes in eruption style.

Geological Observations and Measurements

We made visual observations on the lava dome and sampled 10 blocks containing tuffisites, up to a maximum size of 30 × 30 × 30 cm. These blocks were used to make thin sections of host rock and tuffisite veins for optical microscopy and backscatter electron (BSE) imaging using a Philips XL 30 scanning electron microscope (SEM). Permeability measurements on the host rock and tuffisite veins were made using a TinyPerm II minipermeameter from New England Research Inc. (for details of the assembly, procedure and a discussion of errors see Filomena et al., 2014). Twenty-three permeability measurements were made on the host rock and 27 on the tuffisite veins. Following these measurements, cores of 5 mm (diameter) and 3–7 mm (height) were made from eight locations in the host rock and eight locations in the tuffisites to measure corresponding porosity (from volume and mass measurements) using a Micromeritics He-Pycnometer.

Sintering Pyroclastic Material to Reconstruct Tuffisites

Since the conditions which lead to it, and the processes by which magma fragmentation occurs are relatively well understood (e.g., Alidibirov and Dingwell, 1996; Papale, 1999; Sahagian, 1999; Mueller et al., 2005; Fowler et al., 2010; Arciniega−Ceballos et al., 2015; Cashman and Scheu, 2015; Gonnermann, 2015) our reconstruction of tuffisite formation focuses on the post-deposition sintering of fragmental materials. By recreating the physical properties of tuffisites and applying established sintering models (see Supporting Information for a discussion of competing models) to describe the process we aim to constrain the conditions which form them.

We took a block of lava from the dome of Volcán de Colima and produced a thin section for analysis of interstitial glass composition by wavelength dispersive analysis (WDA) in a CAMECA SX100 SEM. The rest of the material was crushed and sieved to a particle size of 32–350 μm.

This particulate material was then loaded incrementally (1 g at a time, loose and without compaction) into seven 35 mm inner diameter alumina crucibles and filled to a height of 50 mm. The porosity of the unconsolidated samples was calculated using volume and mass measurements of the full and empty crucibles from a Micromeritics He-Pycnometer. In addition, the permeability of the unconsolidated material in each crucible was measured using a New England Research Inc. TinyPerm II minipermeameter.

We then chose our experimental temperature based on the conduit temperature estimate of >940°C (Reubi et al., 2013), rheological work on the dome lavas (Lavallée et al., 2012) and calorimetric measurements on the rhyolitic interstitial glass that show the T_g is 746–751°C (at a cooling rate of 10°C/minute; Kendrick et al., 2013). The samples were then placed into a pre-heated Carbolite 1400 furnace to sinter at a target temperature of either 940 or 980°C for 3, 72, 120, or 168 h and then cooled at 4°C per minute to room temperature (to minimize differential cooling that could cause damage to the sample). The permeability of six sintered samples (72, 120, or 168 h at both temperatures) and porosity of all seven sintered samples was measured before soaking the 168 h, 940°C sample in epoxy and extracting a 10 mm wide core for polishing and examination in an SEM.

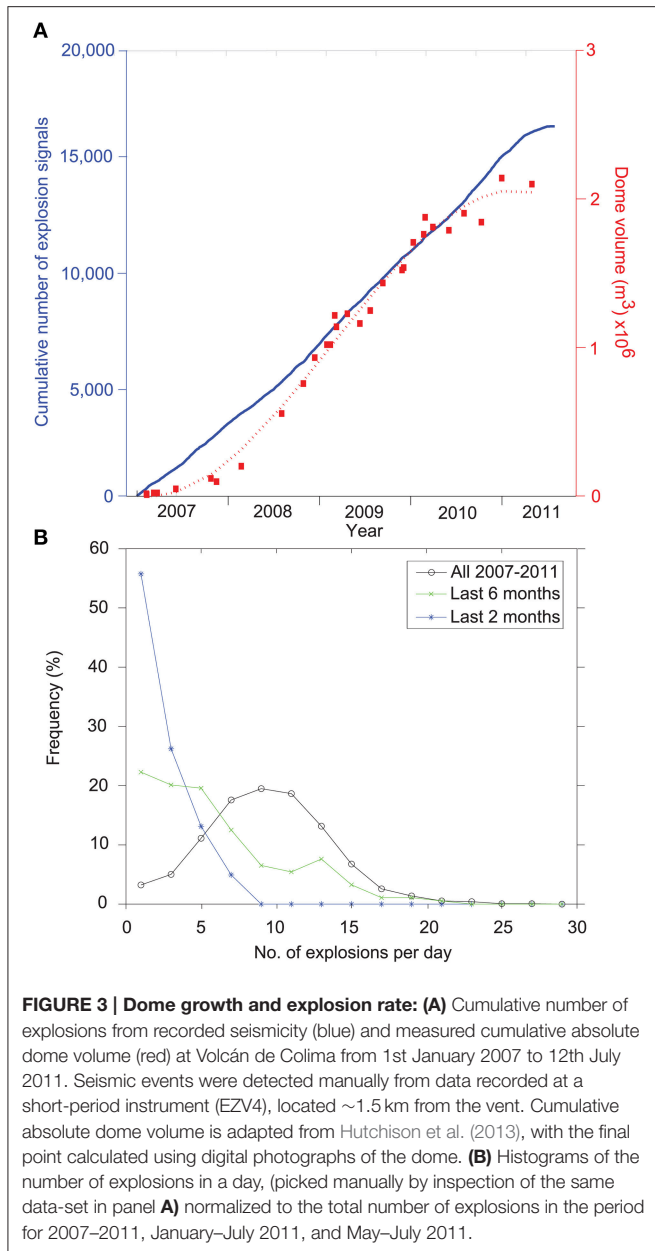## RESULTS

Monitoring

From 2007 to mid-2011 a lava dome grew at Volcán de Colima, punctuated by several thousand small gas and ash explosions (**Figure 2**, insert). Using seismic data recorded at station EZV4 (**Figure 2**) and which were manually classified and counted by CIIV, we can measure the cumulative number of explosion signals recorded in this period (**Figure 3A**). The dome growth was fairly constant, but during the final 6 months of the eruption extrusion rate slowed and the dome volume plateaued (**Figure 3A**). Throughout the dome growth there were, on average, nine explosions per day, but as growth slowed during the last 6 months this decreased, and in the last 2 months there was an average of just one explosion per day (**Figure 3B**). The eruption eventually terminated on 21st June 2011 when there was a larger magnitude explosion which destroyed a small area in the central portion of the dome (James and Varley, 2012). The volcano then entered an exceptional, extended period of quiescence, which lasted until 6th January 2013 and that allowed access to the >2 million m³ lava dome.

Geological Observations and Measurements

Upon accessing the summit of Volcán de Colima on 20th March 2012, it became apparent that a large proportion of blocks on the lava dome contained tuffisites. We traversed around 1/3 of the lava dome surface (**Figure 4A**) and found that in some localized areas (meters to 10's of meters) almost every block contained tuffisite, whereas overall typically 20–40% of the dome blocks contained one or more tuffisites. The tuffisites consisted of 1–30 mm thick veins of moderately consolidated, poorly sorted, pyroclastic ash fragments with varying degrees of oxidization (**Figure 4**). Tuffisites were present in blocks that were between centimeters and meters in size, with cross-cutting veins that depict a repetitively occurring process (**Figure 4B**) and veins that extended laterally up to several meters in some cases.

FIGURE 3 | Dome growth and explosion rate: (A) Cumulative number of explosions from recorded seismicity (blue) and measured cumulative absolute dome volume (red) at Volcán de Colima from 1st January 2007 to 12th July 2011. Seismic events were detected manually from data recorded at a short-period instrument (EZV4), located ∼1.5 km from the vent. Cumulative absolute dome volume is adapted from Hutchison et al. (2013), with the final point calculated using digital photographs of the dome. (B) Histograms of the number of explosions in a day, (picked manually by inspection of the same data-set in panel A) normalized to the total number of explosions in the period for 2007–2011, January–July 2011, and May–July 2011.

On the lava dome, tuffisites were often exposed on the surface of blocks, revealing internal fracture and channel patterns (**Figures 4B–D**). Indeed, the impression was that the blocks had split along the weaker tuffisite veins during disruption of the lava dome, and that the blocks were often defined by these features. Fracture and channel patterns exist in planes of tuffisite, across fracture zones and are characterized by sub-parallel lenses of pyroclastic material with a blocky morphology, which are cross-cut by co-extending channels that excavate the tuffisites and host magma alike (**Figure 4C**). While fracturing of magma can proceed by different mechanisms including shear-fracturing (Gonnermann and Manga, 2003), the field and sample textural evidence here, including the sub-parallel lenses, suggests fragmentation resulting from pore

overpressure and rupture (e.g., Gonnermann, 2015) leading to the propagation of a decompression wave (Fowler et al., 2010). This process is typical of fragmentation of high viscosity magma, and here depicts a layer-by-layer brittle fragmentation process, with each lens representing a fragmentation horizon (**Figures 4C–E**). The co-extending channels (**Figure 4C**) are approximately perpendicular to the elongate, sub-parallel ash lenses, and are themselves free from pyroclastic material, but their negative-relief (even on matching pairs of tuffisites) suggests they may have remained open, forming important fluid transport pathways. Close examination of the fracture and channel patterns on the surface tuffisites reveals that fragmentation must occur as the lava resides at magmatic temperatures, since fractures between the fragmentation horizons in the tuffisite are fluidally backfilled by the host magma (**Figure 4D**). This observation requires that the fracturing of host blocks as well as the tuffisites formed above the glass transition temperature (T_g) of the interstitial melt phase of the host, allowing it to flow into the void left by the fragmentation event. Since the tuffisite veins cross-cut one another, and as the formation must be at temperatures above T_g, we can infer residence times of longer than one explosion cycle at magmatic temperatures.

Further confirmation that tuffisites form and reside at magmatic temperatures is attained by microscopic examination of the internal structures of the tuffisites: all showing brittle to fluidal textures and containing fragmental, angular clasts of crystals and glass that have sintered together (**Figures 4F–H**), a process that can only occur while the melt (interstitial glass) exceeds the glass transition temperature. In addition, prolonged residence times of the tuffisite hosting lava during outgassing are supported by the presence of cristobalite needles in some tuffisites (**Figure 4H**). The presence of cristobalite only in tuffisites and not in the host lavas suggests it is likely to be a product of vapor phase deposition (Horwell et al., 2013), though it can also relate to the devitrification of glass (e.g., Schipper et al., 2015).

In some cases tuffisites appear to be made up of ash transported from elsewhere and deposited into fractures, these veins have sharp boundaries, contain poorly sorted fragments, and there is no continuum between the tuffisite and host-magma textures (**Figure 4F**). However, other tuffisites appear to represent failed or partial fragmentation events locked into the lava in which they initiated; these "failure nuclei" contain angular and sharp fragments ripped from the adjacent magma (**Figure 4G**). Both the failure nuclei examples and the veins which have fragmentation horizons have gradual or graded margins that depict the host rock breaking apart (**Figures 4G,H**).

We explore the influence of the tuffisite veins on the lava by measuring the porosity and permeability of both types of natural sample (**Table 1**). We see that, while the host rock permeability ranged from 10^{-13} to 10^{-15} m², and porosity from 0.10 to 0.14, the tuffisite was typically two orders of magnitude more permeable at 10^{-11}–10^{-14} m² and porosity was more than double at 0.30–0.43 (**Table 1**). Considering the amount of blocks containing tuffisites on the lava dome, the rather more porous and permeable structure exhibited by the tuffisite deserves further attention.
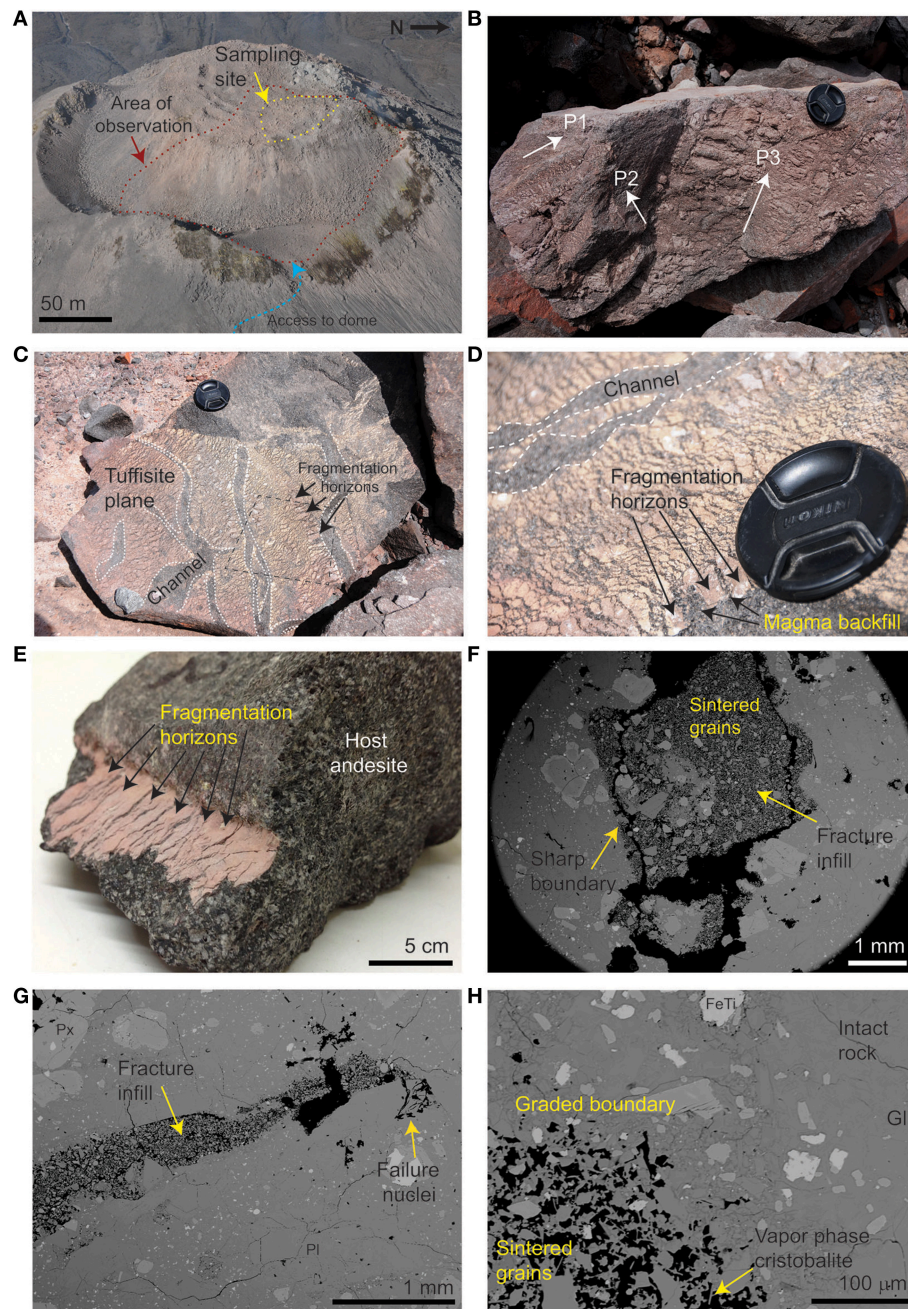
FIGURE 4 | Lava dome samples in detail. (A) Photograph of the Volcán de Colima lava dome on 27th May 2011, a month before the cessation of activity which allowed access to the dome on 20th March 2012, when ~1/3 of the lava dome surface was surveyed (red dashed area) and samples were collected (yellow dashed area). **(B)** 40 cm long block *in situ* on the lava dome with tuffisite on the surface and propagating through the rock in at least three planes (P1, P2, P3; marked with arrows) that cross-cut one another. **(C)** A surface exposure along the plane of the tuffisite, which shows sub-parallel lenses of sintered fragmental material interpreted as fragmentation horizons (marked by black arrows). The tuffisite plane is scoured or excavated by channels (white dashed lines) that host no fragmental material, which are deemed to be outgassing pathways. Dashed box shows area in; **(D)** A zoomed image of the fracture and channel patterns with magma backfill, i.e., the residual structure of the viscous flow of the magma into the fractures between the sintered pyroclastic lenses that make up the fragmentation horizons. **(E)** A tuffisite vein propagating inside a porphyritic Volcán de Colima andesite, again showing sub-parallel fragmentation horizons on the oxidized tuffisite surface. **(F)** BSE image of a tuffisite, here the fracture filled with fragmental material has a sharp contact to the host lava, the fragmental material is rounded to sub-angular and relatively poorly sorted and the tuffisite shows variably sintered zones (denser vs. more porous). **(G)** BSE image of tuffisite in a fracture widening (to the left) from its nucleation point (the failure nuclei) with angular particles caught ripping from the fragmenting host lava, which is otherwise relatively dense. Crystals of plagioclase (Pl) and pyroxene (Px) dominate the phenocrysts assemblage **(H)** BSE image of gradational fracture damage at the boundary of the tuffisite and host lava, where fragment boundaries become increasingly defined toward the tuffisite. Pyroclastic material in the vein is sintered, as indicated by the sub-rounded morphology dictated by the interstitial glass. The tuffisite vein contains needles of vapor phase deposited cristobalite. Phenocrysts of iron-titanium oxides (FeTi) are smaller than plagioclase and pyroxene phenocrysts, and interstitial glass (Gl) is hard to distinguish from plagioclase crystals but is present throughout host rock and tuffisite vein.

TABLE 1 | Measurements of natural host rock and tuffisite samples: Permeability measured by TinyPerm II minipermeameter for blocks 1, 2, 3, 5, and 7, with corresponding porosity measured by helium pycnometry for cores of 5 mm (diameter) and 3–7 mm (height) taken from blocks 1 and 2.

Host rock			Tuffisite		
Block number	Permeability (m^2)*	Porosity$^\#$	Block/tuffisite vein number	Permeability (m^2)*	Porosity$^\#$
1	2.180E-13	0.1239	1/vein 1	3.130E-11	0.3752
1	1.112E-13	0.1151	1/vein 1	2.113E-11	0.3134
1	5.068E-14	0.1125	1/vein 1	4.390E-12	0.3077
1	3.722E-14	0.1081	1/vein 1	3.316E-12	0.2947
1	3.513E-13	–	1/vein 2	9.381E-13	–
1	1.842E-13	–	1/vein 2	8.153E-13	–
1	6.901E-14	–	1/vein 2	7.708E-13	–
1	6.710E-14	–	1/vein 3	6.148E-12	–
1	7.520E-15	–	1/vein 3	2.368E-12	–
1	1.697E-14	–	2/vein 1	3.310E-11	0.4329
2	2.061E-13	0.1373	2/vein 1	1.509E-11	0.3936
2	2.004E-13	0.1347	2/vein 1	5.051E-12	0.3399
2	1.353E-13	0.1239	2/vein 1	3.710E-12	0.3200
2	3.146E-14	0.1034	2/vein 2	2.964E-12	–
2	4.928E-14	–	2/vein 2	2.882E-12	–
2	4.049E-14	–	2/vein 2	2.368E-12	–
3	9.939E-14	–	3/vein 1	8.623E-13	–
3	7.507E-14	–	3/vein 1	5.203E-13	–
3	1.475E-14	–	3/vein 1	3.513E-13	–
3	6.179E-15	–	3/vein 2	8.139E-12	–
5	4.042E-13	–	3/vein 2	6.878E-12	–
5	3.513E-13	–	5/vein 1	2.299E-11	–
7	3.241E-15	–	5/vein 1	1.467E-11	–
			7/vein 1	4.397E-13	–
			7/vein 1	4.276E-13	–
			7/vein 1	2.180E-13	–
			7/vein 1	2.658E-14	–

Each measurement represents a different locality on the sample.

*Error on permeability measurements is quoted by TinyPerm as <0.2 orders of magnitude. $^\#$Error on porosity is estimated to be <0.1% for this sample size.

TABLE 2 | Geochemical oxide composition (%) of quenched interstitial glass measured by wavelength dispersive analysis in a CAMECA SX100 scanning electron microprobe.

Oxide	SiO_2	TiO_2	Al_2O_3	FeO	MnO	MgO	CaO	Na_2O	K_2O	P_2O_5	SO_2	Cl	Cr_2O_3
Mean	77.67	0.62	10.99	1.73	0.03	0.10	0.35	3.31	4.98	0.05	0.01	0.14	0.01
Standard deviation	0.40	0.07	0.26	0.11	0.03	0.04	0.13	0.25	0.26	0.02	0.01	0.02	0.02

Values are the mean of 22 points, normalized to 100%, with standard deviation shown.

Sintered Pyroclastic Material

WDA on the material used for sintering confirmed that the interstitial glass was rhyolite (**Table 2**), and, using the model of Giordano et al. (2008) we found the glass transition temperature (T_g) of 748°C, in keeping with previous calorimetry measurements on dome collapse samples from Volcán de Colima that have shown that the "dry" rhyolitic interstitial glass has a T_g of 746–751°C (Kendrick et al., 2013).

Prior to sintering the granular material, we measured the average porosity of the unconsolidated samples in crucibles to 0.41 (**Table 3**), equating approximately to the predicted maximum loose packing of particles (for a discussion see Torquato and Stillinger, 2002). We also prepared some of the granular material for examination in an SEM, and found that the crushed material captured the coarse fraction of the natural materials well, but fines appeared underrepresented (**Figure 5**). The unconsolidated material loosely packed had an average permeability of 8.8×10^{-10} m^2. Porosity and permeability data show that sintering led to a densification of the samples with increasing time (**Figure 6**). The samples sintered at higher temperature (980°C) became denser and increasingly impervious to gas flow more rapidly than those sintered at lower temperature

TABLE 3 | Measurements of physical properties of synthetic samples: Porosity by He-pycometry for crucibles (35 mm diameter) filled to 50 mm with crushed and sieved andesite before and after sintering at a range of timescales (accurate to the nearest minute) and temperatures, as well as corresponding permeability measurements using a TinyPerm II minipermeameter.

Sample	Sintering timescale (h)	Temperature (±2°C)	Porosity before	Porosity after	Permeability before (m²)	Permeability after (m²)	Standard deviation, permeability after
Crucible 1	3	980	0.4135	0.4098	8.81E-10	Sample broke	Sample broke
Crucible 7	72	980	0.4240	0.4136	9.03E-10	4.701E-11	0.03
Crucible 6	120	980	0.4110	0.3940	8.7E-10	2.536E-11	0.22
Crucible 2	168	980	0.3761	0.3570	8.55E-10	1.397E-11	0.06
Crucible 5	72	940	0.4321	0.4288	9.11E-10	3.081E-10	0.04
Crucible 4	120	940	0.4110	0.4077	8.92E-10	2.139E-10	0.06
Crucible 3	168	940	0.4074	0.4027	8.65E-10	1.346E-10	0.01
Unconsolidated	0	20	0.4107*	—	8.824E-10*	—	—

*Values after are the average of up to four measurements while values before are one measurement only as each crucible is considered a repeat measurement. Error on permeability measurements results from the contact of the permeameter nozzle and sample and is quoted by New England Research Inc. as <0.2 orders of magnitude, while error on porosity is estimated to be <0.1% for this sample size. *The measurements for unconsolidated material are the average of all crucibles prior to sintering.*
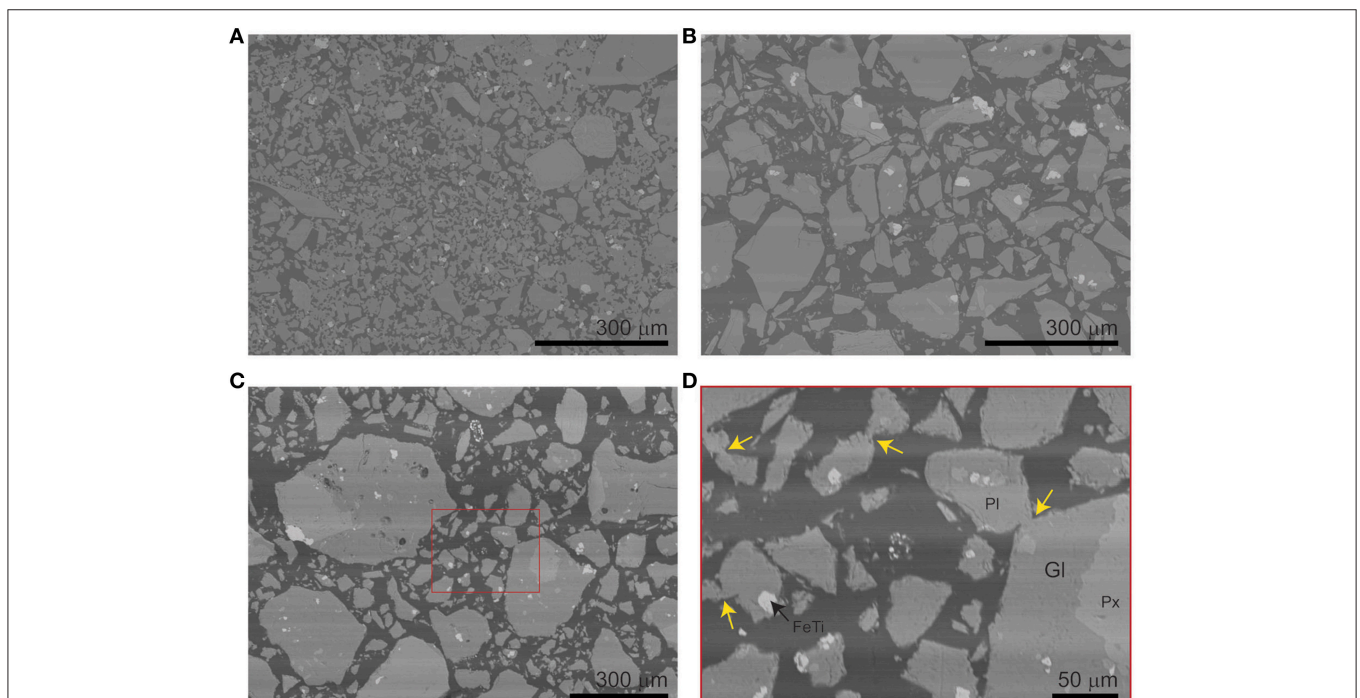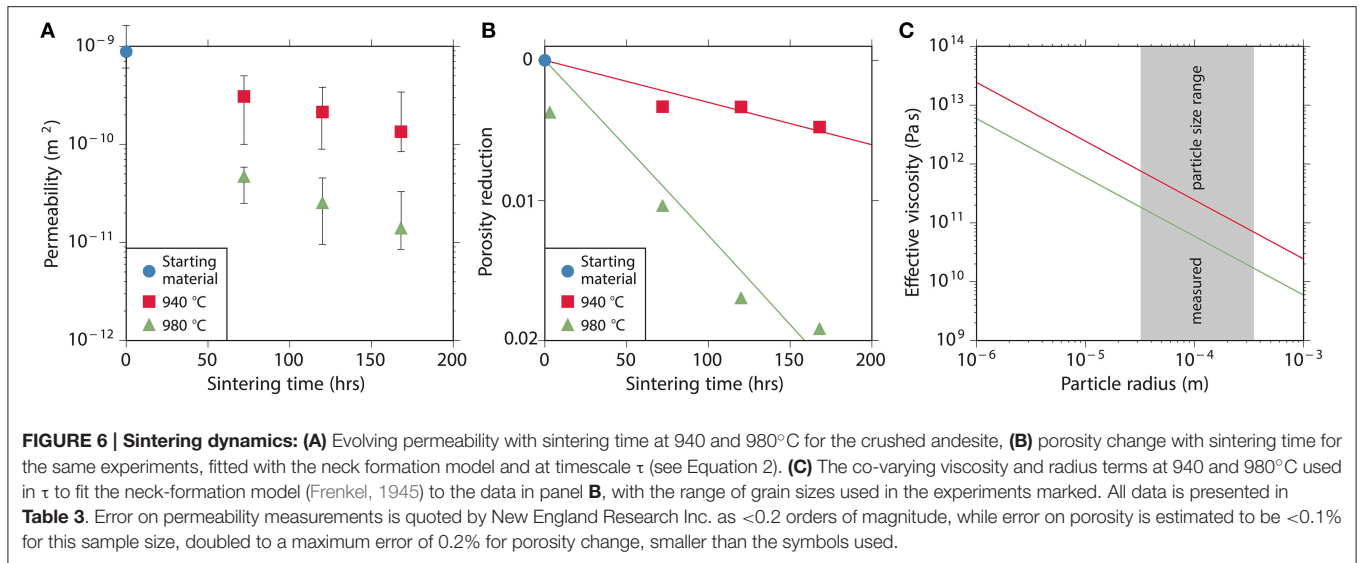

FIGURE 5 | BSE images of natural and experimental samples. (A) Natural tuffisite in a block collected from the Volcán de Colima lava dome on 20th March 2012; **(B)** The crushed dome lava material used for sintering experiments; **(C)** The crushed material after sintering for 168 h at 940°C, showing slight rounding relative to the starting material and highlighting area shown in; **(D)** Closer image of the same sintered sample, highlighting the formation of viscous necks between grains in the interstitial glass (marked by yellow arrows) and with main constituents of the lavas marked: Phenocrysts of pyroxene (Px), iron-titanium oxides (TeTi), and plagioclase (Pl) which is dominant, but difficult to distinguish from interstitial glass (Gl). The 2D section does not allow for a full reconstruction of the sintered particulate network, but sintering is evidently more advanced in the natural material than the experimentally sintered example **(D)**.

(940°C). The 980°C sintered samples had a porosity decrease of <0.02 over 168 h, and permeability decreased by up to two orders of magnitude. In contrast the 940°C samples had a porosity decrease of <0.01 over 168 h, and permeability decreased by just under one order of magnitude (**Table 3**, **Figure 6**). The physical transformation of the samples included an increase in apparent oxidation and consolidation to form a rigid but weak framework, and 2D examination in SEM reveals sintering

contacts still in their infancy as compared to the natural tuffisites (**Figure 5**).

SINTERING DATA ANALYSIS

The sintering process of single-phase melt droplets has previously been explored theoretically, and is relatively well understood, though solutions often include simplifications in the treatment

FIGURE 6 | Sintering dynamics: (A) Evolving permeability with sintering time at 940 and 980°C for the crushed andesite, **(B)** porosity change with sintering time for the same experiments, fitted with the neck formation model and at timescale τ (see Equation 2). **(C)** The co-varying viscosity and radius terms at 940 and 980°C used in τ to fit the neck-formation model (Frenkel, 1945) to the data in panel **B**, with the range of grain sizes used in the experiments marked. All data is presented in **Table 3**. Error on permeability measurements is quoted by New England Research Inc. as <0.2 orders of magnitude, while error on porosity is estimated to be <0.1% for this sample size, doubled to a maximum error of 0.2% for porosity change, smaller than the symbols used.

of particle size, geometry, or their distributions. Here, we model the sintering process whilst including the complexity of natural crystals present in magmas. We confine our analysis to the case where buoyancy forces are negligible compared with surface tension forces. This is captured by the Eötvös number Eo $= \rho g R^2 / \Gamma$ where ρ is the density of particles with a given radius(R), g is the gravitation acceleration, and Γ is the interfacial tension. When Eo $\ll 1$, the model described below can be used.

Sintering of high viscosity liquid droplets, such as silicate melts at magmatic temperatures, have been found to scale with a characteristic timescale across a large range of viscosities (Vasseur et al., 2013; Wadsworth et al., 2014). This is the capillary timescale (τ) defined by Taylor (1934), that describes the relaxation of a droplet to a sphere under the excess surface stress exerted by interfacial tension and is dependent on the particle radius and the Newtonian melt viscosity μ via:

$$\tau \approx \frac{R\mu}{\Gamma} \qquad (1)$$

This scaling for the characteristic timescale is also used in studies interested in the relaxation of a pore in a melt to a spherical geometry under surface tension (e.g., Manga et al., 1998; Llewellin et al., 2002; Kennedy et al., 2016) and was the basis for the sintering model of Frenkel (1945), who considered that the neck formation between touching particles (due to excess surface stresses which act to minimize surface area) was the mechanism by which volume changes occur. To reconstruct tuffisite formation we deal with this initial stage of sintering, in which the permeability reduction is comparatively rapid and the porosity reduction is small (**Figures 6A,B**), so we can apply the neck-formation model (Frenkel, 1945). We verify that neck-formation is the regime of interest in our samples by examining the experimental products in an SEM (**Figures 5C,D**). We scaled the theoretical approximation of Frenkel (1945) up to the bulk

property, porosity (ϕ_g), after Prado et al. (2001), and this takes the form:

$$\phi_g = 1 + \left(\phi_{g,i} - 1\right)\left(1 - \frac{3t}{8\tau}\right)^{-3} \qquad (2)$$

where subscript i denotes initial, and t is the experimental time. During the sintering process the material is thought to transition from a granular mixture of high viscosity droplets to a continuum of high viscosity liquid with a pore network. Once this is the case, the Frenkel (1945) model is unsatisfactory and other models must be implemented (for a discussion see Supporting Information and e.g., Mackenzie and Shuttleworth, 1949; Prado et al., 2001; Wadsworth et al., 2014).

Since the magma at Volcán de Colima is not a simple, single-phase liquid, crystalline phase components must be accounted for in our consideration of the viscosity of the droplets. First, the melt viscosity itself is temperature dependent, which we parameterize by way of a Vogel-Fulcher-Tammann (VFT) equation, $\log_{10}(\mu) = A + B/(T - C)$, where A, B, and C are constants to be determined and T is the temperature. Using the compositional model of Giordano et al. (2008) we find that for the quenched glass composition (**Table 2**) $A = -4.55$, $B = 11939.4$, and $C = 26.55$ (where the temperature term in the VFT equation is in °C). For the sintering temperatures of 940 and 980°C, the melt viscosity predicted by using these parameters is $10^{8.52}$ and $10^{7.97}$ Pa.s, respectively. The effect of crystals is incorporated into the viscosity calculation employed in the sintering timescale using the Maron-Pierce equation for the relative viscosity of a particle suspension, which is well calibrated for magmatic suspensions (Mader et al., 2013):

$$\eta_r = \frac{\eta}{\mu} = \left(1 - \frac{\phi_c}{\phi_m}\right)^{-2} \qquad (3)$$

where η_r is the relative viscosity defined as the effective suspension viscosity (η), relative to the melt viscosity (μ), and crystal volume fraction (ϕ_c) is taken relative to the maximum possible packing of crystals (ϕ_m) in the melt. Determination of ϕ_m depends on the crystal aspect ratio r_p (after Mueller et al., 2010) via the relationship given in Truby et al. (2015):

$$\phi_m \approx \phi_{m0} \exp\left(\frac{-(log_{10}r_p)^2}{2b^2}\right) \qquad (4)$$

Where b is a constant that is ~1.08 for smooth particles or ~1 for rough particles and ϕ_{m0} is the maximum packing of particles that have an aspect ratio of 1 and is ~0.66 or ~0.55 for smooth and rough particles, respectively. As such for $r_p = 1$, $r_p = 2$, or $r_p = 3$ we find that ϕ_m is 0.66, 0.635, and 0.599, respectively, assuming the particles are smooth. Our crystal phase is predominantly plagioclase, with an average r_p-value of 2 (varying from 1 to >3). Therefore, for this analysis, using the Maron-Pierce equation with $\phi_m = 0.635$ we can predict how the melt viscosity is increased as particle fractions are added. While alternative formulations exist for the effect of suspended crystals on magmatic melt viscosities, the simplicity of the Maron-Pierce equation has been thoroughly experimentally validated (e.g., Mueller et al., 2010, 2011; Moitra and Gonnermann, 2015) and is considered valid for the slow viscous sintering process which is limited by the rate of surface-stress driven fluid flow.

As the absolute crystal content and a measure of the suspended crystal aspect ratio distribution are difficult to quantify in these fine-grained powders, we opt to fit Equation (2) to our data by allowing the value of τ to vary freely. We then critically assess whether the fitted value of τ is reasonable for Colima lava. When fitting Equation (2) to our experimental data (**Figure 6B**) we find that in this initial stage of sintering, the Frenkel (1945) model provides a good description of the data.

The fitted values of τ are $10^{3.79}$ and $10^{3.85}$ s for 940 and 980°C, respectively. The physical meaning of τ is described by Equation (1). Since the value for surface tension for "dry" rhyolitic melt is broadly temperature independent and can be approximated to 0.3 N.m^{-1} (Bagdassarov et al., 2000), the other two parameters controlling τ need to be assessed: To arrive at the best-fit τ-values, the viscosity term and radius terms co-vary (Equation 1; **Figure 6C**). This means that for the range of radii measured in our samples the effective viscosity of the sintering particles should be ~$10^{10.2}$−$10^{11.3}$ or ~$10^{10.8}$−$10^{11.9}$ Pa.s for 980 or 940°C, respectively. Using the expression for the temperature dependence of the melt viscosity coupled with Equations (3) and (4), we know that this would equate to a particular crystal volume fraction. Taking an aspect ratio of 2, then to achieve the effective viscosities expected, the crystal volume fraction would have to be ~0.59. This is close to the maximum packing values for those aspect ratios, and corresponds well to the observed crystal fraction in these samples, and previous studies of Colima lavas (e.g., Lavallée et al., 2012; Kendrick et al., 2013; Heap et al., 2014b).

DISCUSSION

Intermittent gas-and-ash explosions occurred throughout the 2007–2011 activity at Volcán de Colima; these explosions became gradually less frequent, decreasing to just one a day in the last 2 months of the eruption. This coincided with a decrease in extrusion rate from late 2010 onwards (**Figure 3**), perhaps as the influx of new magma was balanced by the cooling and contraction of the lava dome, until quiescence began in June 2011, allowing access to the >2 million m^3 lava dome, which provided a unique opportunity to study lava dome structures in detail.

There, we found tuffisites; variably sintered veins of pyroclastic material, which are the product of subsurface fragmentation events. The fracture and channel morphology of the veins and their angular, granular character led to the interpretation that these tuffisite veins represent the *in situ* residue of fragmentation events occurring in the upper conduit and lava dome; fragmentation that occurs during magma ascent as an increase in pore pressure challenges the stability of the magma, which may suffer brittle failure at the glass transition (Alidibirov and Dingwell, 1996; Papale, 1999; Gonnermann, 2015). We can envisage the formation of tuffisites as a 3-step process of: (1) failure, fragmentation, and deposition of fragmental material, (2) sintering and magma backfilling, and (3) excavation and outgassing. This process creates a permeable pathway that allows passive outgassing in that area until magma ascent disrupts it or, if feasible, until sintering of this pyroclastic material (held at magmatic temperatures) slowly closes the permeable pathways. The ubiquitous presence of tuffisites on the andesite lava dome brings into question their scarcity in deposits found downslope and, more broadly, in the rock record; plausibly, tuffisites are destructed during energetic explosive events and transport, and thus their occurrence may in fact be more common than supposed.

The cross-cutting relationships of the veins requires that the tuffisites formed over multiple events, and likewise the exposure of tuffisite veins on block surfaces, including common matching imprints on adjacent surfaces, are a testament to further disruption of the dome (including ongoing magma extrusion and subsequent explosions) that occurred following formation. Since gas loss at Volcán de Colima is predominantly from the summit vent and edifice gas measurements show consistently low emissions (Varley and Taran, 2003) we propose that the incremental formation of these permeable tuffisites helped control the ability of the magma to build overpressure required for explosions.

We can compare the physical attributes of the natural tuffisites and host rocks collected from the lava dome of Volcán de Colima to the sintered samples. The host rock porosity-permeability is bracketed by other porosity-permeability measurements on lavas from Volcán de Colima (Kendrick et al., 2013; Farquharson et al., 2015), and is akin to measurements on other lavas from basaltic (Schaefer et al., 2015) to dacitic (Mueller et al., 2005) to rhyolitic (Heap et al., 2014a; Okumura and Sasaki, 2014). The trend in porosity-permeability data is well described by the relationship given for effusive lavas in Mueller et al. (2005), as is

the majority of the natural tuffisite, with some examples falling into a range that is slightly more permeable than anticipated from their porosity (**Figure 7**). Meanwhile, the granular, crushed dome material falls well outside of this porosity-permeability relationship, being almost 2 orders of magnitude more permeable than expected for the given porosity, and the sintered samples bridge the void between the loose packed fragments and the porosity-permeability of the lava samples.

Here, we show that the surface tension dominated sintering process for the crystalline andesite is capable of recreating the porosity-permeability of natural tuffisite on the order of several weeks. We can see that our sintered samples begin to exhibit similar internal structures to the natural tuffisites (**Figure 5A**), including the presence of viscous necks between grains (**Figures 5C,D**). This process is effectively described using the neck formation model of Frenkel (1945), which explains the permeability-porosity reduction as this process reduces connectivity. Neck formation during the experimental sintering

process appears to more significantly alter the permeability than the porosity, in fact, theory states that the neck formation model is ineffective below 0.32 porosity (Prado et al., 2001; Rahaman, 2008). This matches our observation that the trajectory of decreasing porosity-permeability during sintering intercepts the zone of porosity-permeability for effusive lavas (after Mueller et al., 2005) at approximately this value (**Figure 7**). It also supports the hypothesis that during sintering, material transitions from a granular mixture of high viscosity droplets to a continuum of high viscosity liquid with a pore network. Permeability reduction is most rapid at the onset of sintering, prior to this transition, and while the neck formation model of Frenkel (1945) is applicable. We find that the porosity-permeability relationship of lavas from Mueller et al. (2005) is only applicable beyond this transition, where there is a change-in-slope of the porosity-permeability plot.

In our data the intercept, or change-in-slope, marks the location of the natural tuffisites in terms of porosity-permeability,
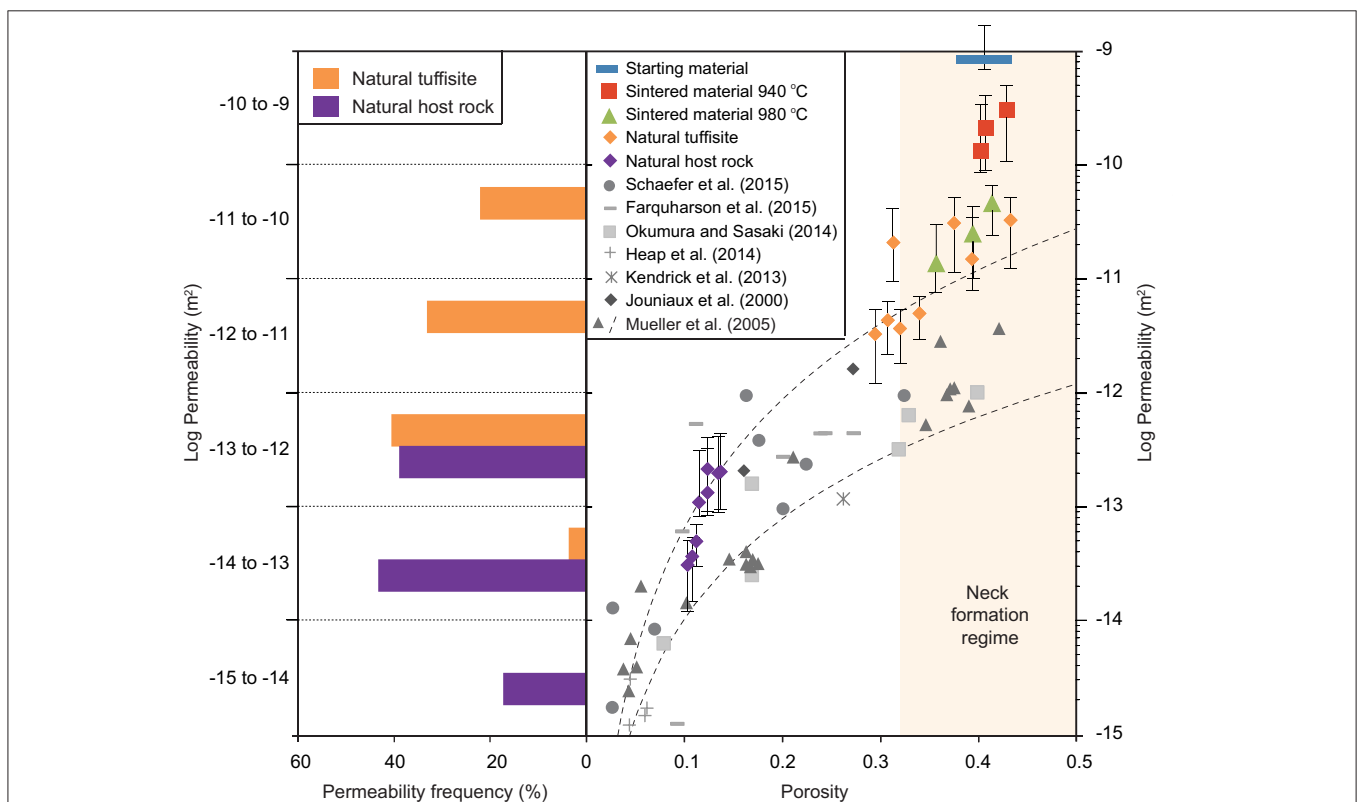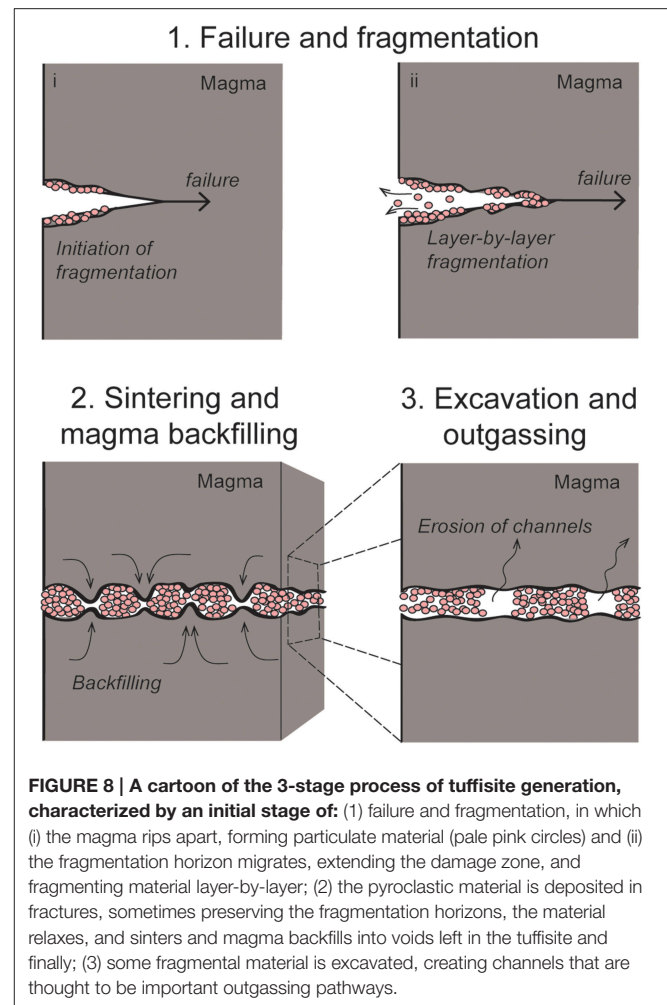

FIGURE 7 | Physical attributes of natural tuffisites, their host rocks and the crushed and sintered analogs: On the left, the permeability distribution (%) for natural materials, calculated from 23 host rock and 27 tuffisite vein permeability measurements made using the TinyPerm II minipermeameter. Following these measurements, cores of 5 mm (diameter) and 3–7 mm (height) were made from eight locations in the host rock and eight locations in the tuffisites to measure corresponding porosity using a He-pycnometer. All data is presented in **Table 1**. On the right, this porosity and permeability relationship for the eight samples of both the natural host rock and tuffisite veins are compared to the crushed dome material and sintered tuffisite analogs from 940 to 980°C (data in **Table 3**). This is compared to porosity—permeability measurements on other lavas from Volcán de Colima (Kendrick et al., 2013; Farquharson et al., 2015) and to lavas from elsewhere ranging from basalt (Pacaya; Schaefer et al., 2015) to dacite (Mount Unzen; Mueller et al., 2005) rhyolite (Mount Meagre; Heap et al., 2014a) and in addition it is compared to the results of compaction experiments on chips of rhyolite lava (Okumura and Sasaki, 2014) and overlain by the porosity–permeability relationship for effusive lava given by Mueller et al. (2005). The plot shows the region in which the neck-formation regime is active, i.e., the region in which sintering materials plot, but where they do not follow the anticipated porosity–permeability trend for lavas. Error on permeability measurements is quoted by New England Research Inc. as <0.2 orders of magnitude, while error on porosity is estimated to be <0.1% for this sample size.

and provides us a constraint for sintering timescale of the natural materials of ~1 week (at the higher experimental temperature of 980°C) to several weeks (at 940°C). However, taking a crystal content of ~0.6, at our experimental conditions the time to almost fully seal porosity could be months to years, and considerably longer at lower temperature, in comparison to pure melts in granular form which can sinter to a negligible porosity in a matter of hours (see Supporting Information; Vasseur et al., 2013). We note that, when magmas are welded during compression (applied force), such as in the study of Okumura and Sasaki (2014), porosity and permeability reduce more readily and the porosity-permeability relationship more closely resembles typical lavas as opposed to natural tuffisites, having lower permeability for a given porosity. Hence, complete healing and closure of the permeable pathways in these crystal-rich magmas, to the point of the host rock, is infeasible at the conditions experienced by the tuffisites studied here (i.e., in the lava dome without confinement and/or high shear stresses). Confining pressure may have played a role in the formation of tuffisites examined by Kolzenburg et al. (2012) collected from block and ash flows at Volcán de Colima, produced mainly from the column collapses of larger Vulcanian explosions in 2005; these tuffisites were much more impervious, but also scarcer than those observed on the dome in 2012. The fragility of tuffisites observed on the lava dome indicates that they may be destroyed during energetic transportation, hence only the strongest tuffisites are represented in pyroclastic deposits and in the rock record.

IMPLICATIONS FOR LAVA DOME LONGEVITY

In concert, our observations suggest that the persistent explosive activity throughout 2007–2011 led to the repeated formation of tuffisites in the upper conduit and lava dome. These explosions formed a permeable network of tuffisites that allowed passive outgassing, as evidenced by secondary cristobalite deposited in the tuffisite veins that is not observed in the host magma. We can summarize the tuffisite formation cycle as (1) failure, fragmentation, and deposition of fragmental material, (2) sintering and magma backfilling, and (3) excavation and outgassing (**Figure 8**). Residence times of the tuffisites were insufficient to recover the impervious character of the host lavas, so outgassing ensued until fresh ascending magma repeatedly replaced the tuffisite-hosting lavas: This less permeable magma allowed the pressure build-up required for further small Vulcanian explosions that created new batches of tuffisites. As extrusion rate waned in the later stages of the eruption the fresh magma replenishment rate slowed, leaving the tuffisites *in situ* for longer, and due to the inability to build pressure, increased the interval between explosions. This slow extrusion rate left the dome riddled with tuffisites in the latter stages of activity. A larger, final explosion occurred on 21st June 2011, which exploited heterogeneities in the lava dome (James and Varley, 2012) and which likely drew upon pressurized gases from deeper in the magma column (e.g., Papale, 1999).

FIGURE 8 | A cartoon of the 3-stage process of tuffisite generation, characterized by an initial stage of: (1) failure and fragmentation, in which (i) the magma rips apart, forming particulate material (pale pink circles) and (ii) the fragmentation horizon migrates, extending the damage zone, and fragmenting material layer-by-layer; (2) the pyroclastic material is deposited in fractures, sometimes preserving the fragmentation horizons, the material relaxes, and sinters and magma backfills into voids left in the tuffisite and finally; (3) some fragmental material is excavated, creating channels that are thought to be important outgassing pathways.

When extrusion subsequently stopped, the permeable tuffisite network was then left in place and the diminishing gas supply could bleed passively, which steered the eruption into an 18 month hiatus. The observations documented here further our understanding of Vulcanian explosion generation and degassing and outgassing processes for these smaller eruptions, and aids in the interpretation of the evolution of activity during prolonged effusion/explosion phases, a critical step for the assessment of associated hazards.

CONCLUSIONS

- Tuffisites formed in the lava dome and upper conduit at Volcán de Colima show a range of viscous to brittle features, but all retain evidence of sintering of viscous particles in cracks and voids.
- We relate the tuffisite formation to Vulcanian explosions occurring >daily, but reducing in rate in the 4 years preceding the onset of quiescence that allowed access to the dome in 2012.
- Natural tuffisites are ~2 orders of magnitude more permeable than the andesitic dome lavas in which they are hosted.

- We can recreate the tuffisites by sintering natural, crystalline, crushed dome lava for different timescales at magmatic temperatures.
- The porosity and permeability reduction during sintering is a result of the formation of viscous necks between adjacent particles, a process effectively described by the neck formation model of Frenkel (1945) down to a porosity of ~0.32.
- The viscous necks form as the interstitial glass (melt), held above the glass transition temperature is able to relax and succumb to surface tension. This study represents the first examination of this process in crystalline lavas.
- During neck formation permeability is influenced more significantly than porosity and the granular material is led back toward the regime anticipated for effusive lavas, a regime that amply describes the andesitic host and the most impervious of the natural tuffisites.
- The recreation of tuffisites in the laboratory provides a constraint on the timescale of formation of the natural tuffisites on the order of several weeks, dependent upon formation temperature.
- It can be inferred that the presence of tuffisite locally increases the permeability on lava domes, indeed, cristobalite deposited in voids in the tuffisites further suggest they may be important outgassing pathways.
- The creation of such a permeable degassing pathway in the lava dome and upper conduit could allow for

degassing that would negate the build-up of pressure required to produce Vulcanian explosions, explaining why event rate waned. This passive bleeding of volatiles could have steered the eruption toward the observed 18-month hiatus.

AUTHOR CONTRIBUTIONS

JK, YL, and NV conceptualized the idea, and conducted fieldwork along with JV. JK and YL performed experiments and measurements, OL processed seismic data while FW and JV modeled the experimental data. JK prepared all data and wrote the manuscript, to which all authors have contributed.

FUNDING

ACKNOWLEDGMENTS

REFERENCES

Alidibirov, M., and Dingwell, D. B. (1996). Magma fragmentation by rapid decompression. *Nature* 380, 146–148. doi: 10.1038/380146a0

Arámbula-Mendoza, R., Lesage, P., Valdés-González, C., Varley, N. R., Reyes-Dávila, G., and Navarro, C. (2011). Seismic activity that accompanied the effusive and explosive eruptions during the 2004-2005 period at Volcán de Colima, Mexico. *J. Volcanol. Geotherm. Res.* 205, 30–46. doi: 10.1016/j.jvolgeores.2011.02.009

Arciniega−Ceballos, A., Alatorre−Ibargüengoitia, M., Scheu, B., and Dingwell, D. (2015). Analysis of source characteristics of experimental gas burst and fragmentation explosions generated by rapid decompression of volcanic rocks. *J. Geophys. Res. Solid Earth* 120, 5104–5116. doi: 10.1002/2014jb011810

Bagdassarov, N., Dorfman, A., and Dingwell, D. B. (2000). Effect of alkalis, phosphorus, and water on the surface tension of haplogranite melt. *Am. Mineral.* 85, 33–40. doi: 10.2138/am-2000-0105

Berlo, K., Tuffen, H., Smith, V. C., Castro, J. M., Pyle, D. M., Mather, T. A., et al. (2013). Element variations in rhyolitic magma resulting from gas transport. *Geochim. Cosmochim. Acta* 121, 436–451. doi: 10.1016/j.gca.2013.07.032

Blundy, J., Cashman, K., and Humphreys, M. (2006). Magma heating by decompression-driven crystallization beneath andesite volcanoes. *Nature* 443, 76–80. doi: 10.1038/nature05100

Burgisser, A., and Degruyter, W. (2015). "Chapter 11; Magma ascent and degassing at shallow levels," in *Encyclopedia of Volcanoes, 2nd Edn.*, eds H. Sigurdsson, B. Houghton, H. Rymer, J. Stix and S. McNutt (Amsterdam: Elsevier), 225–238.

Cashman, C., and Scheu, B. (2015). "Chapter 25; Magmatic fragmentation," in *Encyclopedia of Volcanoes, 2nd Edn.*, eds H. Sigurdsson, B. Houghton, H. Rymer, J. Stix and S. McNutt (Amsterdam: Elsevier), 459–471.

Cashman, K., and Blundy, J. (2000). Degassing and crystallization of ascending andesite and dacite. *Philos. Trans. R. Soc. Lond. A Math. Phys. Eng. Sci.* 358, 1487–1513. doi: 10.1098/rsta.2000.0600

Castro, J. M., Bindeman, I. N., Tuffen, H., and Ian Schipper, C. (2014). Explosive origin of silicic lava: textural and –H_2O evidence for pyroclastic degassing during rhyolite effusion. *Earth Planet. Sci. Lett.* 405, 52–61. doi: 10.1016/j.epsl.2014.08.012

Castro, J. M., Cordonnier, B., Tuffen, H., Tobin, M. J., Puskar, L., Martin, M. C., et al. (2012). The role of melt-fracture degassing in defusing explosive rhyolite eruptions at volcán Chaitén. *Earth Planet. Sci. Lett.* 333–334, 63–69. doi: 10.1016/j.epsl.2012.04.024

Chouet, B. A. (1996). Long-period volcano seismicity: its source and use in eruption forecasting. *Nature* 380, 309–316. doi: 10.1038/380309a0

Chouet, B. A., and Matoza, R. S. (2013). A multi-decadal view of seismic methods for detecting precursors of magma movement and eruption. *J. Volcanol. Geotherm. Res.* 252, 108–175. doi: 10.1016/j.jvolgeores.2012.11.013

Cloos, H. (1941). Bau und taetigkeit von tuffschloten; Untersuchungen an dem schwaebischen vulkan. *Geol. Rundsch.* 32, 709–800. doi: 10.1007/BF01801913

Dingwell, D. B. (1996). Volcanic dilemma: flow or blow? *Science* 273, 1054–1055. doi: 10.1126/science.273.5278.1054

Farquharson, J., Heap, M. J., Varley, N. R., Baud, P., and Reuschlé, T. (2015). Permeability and porosity relationships of edifice-forming andesites: a combined field and laboratory study. *J. Volcanol. Geotherm. Res.* 297, 52–68. doi: 10.1016/j.jvolgeores.2015.03.016

Filomena, C., Hornung, J., and Stollhofen, H. (2014). Assessing accuracy of gas-driven permeability measurements: a comparative study of diverse Hassler-cell and probe permeameter devices. *Solid Earth* 5, 1–11. doi: 10.5194/se-5-1-2014

Fowler, A. C., Scheu, B., Lee, W. T., and McGuinness, M. J. (2010). A theoretical model of the explosive fragmentation of vesicular magma. *Proc. R. Soc. Lond. A Math. Phys. Eng. Sci.* 466, 731–752. doi: 10.1098/rspa.2009.0382

Frenkel, J. (1945). Viscous flow of crystalline bodies under the action of surface tension. *J. Phys.* 9, 385–391.

Gavilanes-Ruiz, J. C., Cuevas-Muñiz, A., Varley, N., Gwynne, G., Stevenson, J., Saucedo-Girón, R., et al. (2009). Exploring the factors that influence the

perception of risk: the case of Volcán de Colima, Mexico. *J. Volcanol. Geotherm. Res.* 186, 238–252. doi: 10.1016/j.jvolgeores.2008.12.021

Giordano, D., Russell, J. K., and Dingwell, D. B. (2008). Viscosity of magmatic liquids: a model. *Earth Planet. Sci. Lett.* 271, 123–134. doi: 10.1016/j.epsl.2008.03.038

Gonnermann, H. M. (2015). Magma fragmentation. *Annu. Rev. Earth Planet. Sci.* 43, 431–458. doi: 10.1146/annurev-earth-060614-105206

Gonnermann, H. M., and Manga, M. (2003). Explosive volcanism may not be an inevitable consequence of magma fragmentation. *Nature* 426, 432–435. doi: 10.1038/nature02138

Green, D. N., and Neuberg, J. (2006). Waveform classification of volcanic low-frequency earthquake swarms and its implication at Soufrière Hills Volcano, Montserrat. *J. Volcanol. Geotherm. Res.* 153, 51–63. doi: 10.1016/j.jvolgeores.2005.08.003

Heap, M. J., Kolzenburg, S., Russell, J. K., Campbell, M. E., Welles, J., Farquharson, J. I., et al. (2014a). Conditions and timescales for welding block-and-ash flow deposits. *J. Volcanol. Geotherm. Res.* 289, 202–209. doi: 10.1016/j.jvolgeores.2014.11.010

Heap, M. J., Lavallée, Y., Petrakova, L., Baud, P., Reuschlé, T., Varley, N. R., et al. (2014b). Microstructural controls on the physical and mechanical properties of edifice-forming andesites at Volcán de Colima, Mexico. *J. Geophys. Res. Solid Earth* 119, 2925–2963. doi: 10.1002/2013JB010521

Horwell, C., Williamson, B., Llewellin, E., Damby, D., and Blond, J. (2013). The nature and formation of cristobalite at the Soufrière Hills volcano, Montserrat: implications for the petrology and stability of silicic lava domes. *Bull. Volcanol.* 75, 1–19. doi: 10.1007/s00445-013-0696-3

Hutchison, W., Varley, N., Pyle, D. M., Mather, T. A., and Stevenson, J. A. (2013). Airborne thermal remote sensing of the Volcán de Colima (Mexico) lava dome from 2007 to 2010. *Geol. Soc. Lond. Spec. Publ.* 380, 203–228. doi: 10.1144/SP380.8

James, M. R., and Varley, N. (2012). Identification of structural controls in an active lava dome with high resolution DEMs: Volcán de Colima, Mexico. *Geophys. Res. Lett.* 39, L22303. doi: 10.1029/2012GL054245

Kendrick, J. E., Lavallée, Y., Hess, K. U., Heap, M. J., Gaunt, H. E., Meredith, P. G., et al. (2013). Tracking the permeable porous network during strain-dependent magmatic flow. *J. Volcanol. Geotherm. Res.* 260, 117–126. doi: 10.1016/j.jvolgeores.2013.05.012

Kendrick, J. E., Lavallée, Y., Hirose, T., Di Toro, G., Hornby, A., De Angelis, S., et al. (2014). Volcanic drumbeat seismicity caused by stick-slip motion and magmatic frictional melting. *Nat. Geosci.* 7, 438–442. doi: 10.1038/ngeo2146

Kennedy, B. M., Wadsworth, F. B., Vasseur, J., Ian Schipper, C., Mark Jellinek, A., Von Aulock, F. W., et al. (2016). Surface tension driven processes densify and retain permeability in magma and lava. *Earth Planet. Sci. Lett.* 433, 116–124. doi: 10.1016/j.epsl.2015.10.031

Kolzenburg, S., Heap, M. J., Lavallée, Y., Russell, J. K., Meredith, P. G., and Dingwell, D. B. (2012). Strength and permeability recovery of tuffisite-bearing andesite. *Solid Earth* 3, 191–198. doi: 10.5194/se-3-191-2012

Lamb, O. D., Varley, N. R., Mather, T. A., Pyle, D. M., Smith, P. J., and Liu, E. J. (2014). Multiple timescales of cyclical behaviour observed at two dome-forming eruptions. *J. Volcanol. Geotherm. Res.* 284, 106–121. doi: 10.1016/j.jvolgeores.2014.07.013

Lavallée, Y., Dingwell, D. B., Johnson, J. B., Cimarelli, C., Hornby, A. J., Kendrick, J. E., et al. (2015). Thermal vesiculation during volcanic eruptions. *Nature* 528, 544–547. doi: 10.1038/nature16153

Lavallée, Y., Varley, N., Alatorre-Ibargüengoitia, M., Hess, K. U., Kueppers, U., Mueller, S., et al. (2012). Magmatic architecture of dome-building eruptions at Volcán de Colima, Mexico. *Bull. Volcanol.* 74, 249–260. doi: 10.1007/s00445-011-0518-4

Llewellin, E. W., Mader, H. M., and Wilson, S. D. R. (2002). The constitutive equation and flow dynamics of bubbly magmas. *Geophys. Res. Lett.* 29, 2170. doi: 10.1029/2002GL015697

Luhr, J. F. (2002). Petrology and geochemistry of the 1991 and 1998-1999 lava flows from Volcán de Colima, México: implications for the end of the current eruptive cycle. *J. Volcanol. Geotherm. Res.* 117, 169–194. doi: 10.1016/S0377-0273(02)00243-3

Luhr, J. F., and Carmichael, I. S. E. (1980). The colima Volcanic complex, Mexico. *Contrib. Mineral. Petrol.* 71, 343–372. doi: 10.1007/BF00374707

Mackenzie, J. K., and Shuttleworth, R. (1949). A phenomenological theory of sintering. *Proc. Phys. Soc. B* 62, 833. doi: 10.1088/0370-1301/62/12/310

Mader, H., Llewellin, E., and Mueller, S. (2013). The rheology of two-phase magmas: a review and analysis. *J. Volcanol. Geotherm. Res.* 257, 135–158. doi: 10.1016/j.jvolgeores.2013.02.014

Manga, M., Castro, J., Cashman, K. V., and Loewenberg, M. (1998). Rheology of bubble-bearing magmas. *J. Volcanol. Geotherm. Res.* 87, 15–28. doi: 10.1016/S0377-0273(98)00091-2

Moitra, P., and Gonnermann, H. M. (2015). Effects of crystal shape- and size-modality on magma rheology. *Geochem. Geophys. Geosyst.* 16, 1–26. doi: 10.1002/2014GC005554

Mora, J. C., Macìas, J. L., Saucedo, R., Orlando, A., Manetti, P., and Vaselli, O. (2002). Petrology of the 1998–2000 products of Volcán de Colima, México. *J. Volcanol. Geotherm. Res.* 117, 195–212. doi: 10.1016/S0377-0273(02)00244-5

Mueller, S., Llewellin, E. W., and Mader, H. M. (2010). The rheology of suspensions of solid particles. *Proc. R. Soc. Lond. A Math. Phys. Eng. Sci.* 466, 1201–1228. doi: 10.1098/rspa.2009.0445

Mueller, S., Llewellin, E. W., and Mader, H. M. (2011). The effect of particle shape on suspension viscosity and implications for magmatic flows. *Geophys. Res. Lett.* 38, L13316. doi: 10.1029/2011GL047167

Mueller, S., Melnik, O., Spieler, O., Scheu, B., and Dingwell, D. B. (2005). Permeability and degassing of dome lavas undergoing rapid decompression: an experimental determination. *Bull. Volcanol.* 67, 526–538. doi: 10.1007/s00445-004-0392-4

Neuberg, J. (2000). Characteristics and causes of shallow seismicity in andesite volcanoes. *Philos. Trans. R. Soc. Lond. A Math. Phys. Eng. Sci.* 358, 1533–1546. doi: 10.1098/rsta.2000.0602

Neuberg, J. W., Tuffen, H., Collier, L., Green, D., Powell, T., and Dingwell, D. (2006). The trigger mechanism of low-frequency earthquakes on Montserrat. *J. Volcanol. Geotherm. Res.* 153, 37–50. doi: 10.1016/j.jvolgeores.2005.08.008

Noguchi, S., Toramaru, A., and Nakada, S. (2008). Groundmass crystallization in dacite dykes taken in Unzen Scientific Drilling Project (USDP-4). *J. Volcanol. Geotherm. Res.* 175, 71–81. doi: 10.1016/j.jvolgeores.2008.03.037

Okumura, S., and Sasaki, O. (2014). Permeability reduction of fractured rhyolite in volcanic conduits and its control on eruption cyclicity. *Geology* 42, 843–846. doi: 10.1130/G35855.1

Palo, M., Ibáñez, J. M., Cisneros, M., Bretón, M., Del Pezzo, E., Ocaña, E., et al. (2009). Analysis of the seismic wavefield properties of volcanic explosions at Volcán de Colima, México: insights into the source mechanism. *Geophys. J. Int.* 177, 1383–1398. doi: 10.1111/j.1365-246X.2009.04134.x

Papale, P. (1999). Strain-induced magma fragmentation in explosive eruptions. *Nature* 397, 425–428. doi: 10.1038/17109

Prado, M., Dutra Zanotto, E., and Müller, R. (2001). Model for sintering polydispersed glass particles. *J. Non Cryst. Solids* 279, 169–178. doi: 10.1016/S0022-3093(00)00399-9

Rahaman, M. N. (2008). *Sintering of Ceramics.* Boca Raton, FL: CRC Press.

Reubi, O., and Blundy, J. (2008). Assimilation of plutonic roots, formation of high-K 'exotic' melt inclusions and genesis of Andesitic Magmas at Volcán De Colima, Mexico. *J. Petrol.* 49, 2221–2243. doi: 10.1093/petrology/egn066

Reubi, O., Blundy, J., and Varley, N. (2013). Volatiles contents, degassing and crystallisation of intermediate magmas at Volcan de Colima, Mexico, inferred from melt inclusions. *Contrib. Mineral. Petrol.* 165, 1087–1106. doi: 10.1007/s00410-013-0849-6

Sahagian, D. (1999). Volcanology - Magma fragmentation in eruptions. *Nature* 402, 589. doi: 10.1038/45099

Sahetapy-Engel, S. T., Harris, A. J. L., and Marchetti, E. (2008). Thermal, seismic and infrasound observations of persistent explosive activity and conduit dynamics at Santiaguito lava dome, Guatemala. *J. Volcanol. Geotherm. Res.* 173, 1–14. doi: 10.1016/j.jvolgeores.2007.11.026

Savov, I. P., Luhr, J. F., and Navarro-Ochoa, C. (2008). Petrology and geochemistry of lava and ash erupted from Volcán Colima, Mexico, during 1998–2005. *J. Volcanol. Geotherm. Res.* 174, 241–256. doi: 10.1016/j.jvolgeores.2008.02.007

Schaefer, L. N., Kendrick, J. E., Lavallée, Y., Oommen, T., and Chigna, G. (2015). Geomechanical rock properties of a basaltic volcano. *Front. Earth Sci.* 3:29. doi: 10.3389/feart.2015.00029

Schipper, C. I., Castro, J. M., Tuffen, H., James, M. R., and How, P. (2013). Shallow vent architecture during hybrid explosive–effusive activity at Cordón Caulle

(Chile, 2011–12): evidence from direct observations and pyroclast textures. *J. Volcanol. Geotherm. Res.* 262, 25–37. doi: 10.1016/j.jvolgeores.2013.06.005

Schipper, C. I., Castro, J. M., Tuffen, H., Wadsworth, F. B., Chappell, D., Pantoja, A. E., et al. (2015). Cristobalite in the 2011–2012 Cordón Caulle eruption (Chile). *Bull. Volcanol.* 77, 1–19. doi: 10.1007/s00445-015-0925-z

Sparks, R. S. J. (1997). Causes and consequences of pressurisation in lava dome eruptions. *Earth Planet. Sci. Lett.* 150, 177–189. doi: 10.1016/S0012-821X(97)00109-X

Stasiuk, M. V., Barclay, J., Carroll, M. R., Jaupart, C., Ratté, J. C., Sparks, R. S. J., et al. (1996). Degassing during magma ascent in the Mule Creek vent (USA). *Bull. Volcanol.* 58, 117–130. doi: 10.1007/s004450050130

Taylor, G. I. (1934). The formation of emulsions in definable fields of flow. *Proc. R. Soc. Lond. A Math. Phys. Eng. Sci.* 146, 501–523. doi: 10.1098/rspa.1934.0169

Thomas, M. E., and Neuberg, J. (2012). What makes a volcano tick—A first explanation of deep multiple seismic sources in ascending magma. *Geology* 40, 351–354. doi: 10.1130/G32868.1

Torquato, S., and Stillinger, F. H. (2002). Controlling the short-range order and packing densities of many-particle systems. *J. Phys. Chem. B* 106, 11406–11406. doi: 10.1021/jp022019p

Truby, J. M., Mueller, S. P., Llewellin, E. W., and Mader, H. M. (2015). The rheology of three-phase suspensions at low bubble capillary number. *Proc. R. Soc. Lond. A Math. Phys. Eng. Sci.* 471:20140557. doi: 10.1098/rspa.2014.0557

Tuffen, H., and Dingwell, D. (2005). Fault textures in volcanic conduits: evidence for seismic trigger mechanisms during silicic eruptions. *Bull. Volcanol.* 67, 370–387. doi: 10.1007/s00445-004-0383-5

Tuffen, H., Dingwell, D. B., and Pinkerton, H. (2003). Repeated fracture and healing of silicic magma generate flow banding and earthquakes? *Geology* 31, 1089–1092. doi: 10.1130/G19777.1

Varley, N., Arámbula-Mendoza, R., Reyes-Dávila, G., Sanderson, R., and Stevenson, J. (2010). Generation of Vulcanian activity and long-period seismicity at Volcán de Colima, Mexico. *J. Volcanol. Geotherm. Res.* 198, 45–56. doi: 10.1016/j.jvolgeores.2010.08.009

Varley, N. R., and Taran, Y. (2003). Degassing processes of Popocatépetl and Volcán de Colima, Mexico. *Geol. Soc. Lond. Spec. Publ.* 213, 263–280. doi: 10.1144/GSL.SP.2003.213.01.16

Vasseur, J., Wadsworth, F. B., Lavallée, Y., Hess, K.-U., and Dingwell, D. B. (2013). Volcanic sintering: timescales of viscous densification and strength recovery. *Geophys. Res. Lett.* 40, 5658–5664. doi: 10.1002/2013GL058105

Voight, B., Sparks, R. S., Miller, A. D., Stewart, R. C., Hoblitt, R. P., Clarke, A., et al. (1999). Magma flow instability and cyclic activity at Soufriere Hills Volcano, Montserrat, British West Indies. *Science* 283, 1138–1142. doi: 10.1126/science.283.5405.1138

Wadsworth, F. B., Vasseur, J., Von Aulock, F. W., Hess, K.-U., Scheu, B., Lavallée, Y., et al. (2014). Non-isothermal viscous sintering of volcanic ash. *J. Geophys. Res. Solid Earth* 119, 8792–8804. doi: 10.1002/2014JB011453

Watts, R. B., Herd, R. A., Sparks, R. S. J., and Young, S. R. (2002). Growth patterns and emplacement of the andesitic lava dome at Soufrière Hills Volcano, Montserrat. *Geol. Soc. Lond. Mem.* 21, 115–152. doi: 10.1144/GSL.MEM.2002.021.01.06

Webb, E. B., Varley, N. R., Pyle, D. M., and Mather, T. A. (2014). Thermal imaging and analysis of short-lived Vulcanian explosions at Volcán de Colima, Mexico. *J. Volcanol. Geotherm. Res.* 278–279, 132–145. doi: 10.1016/j.jvolgeores.2014.03.013

Webb, S. L., and Dingwell, D. B. (1990). Non-Newtonian rheology of igneous melts at high stresses and strain rates: experimental results for rhyolite, andesite, basalt and nephelinite. *J. Geophys. Res.* 95, 15695–15701. doi: 10.1029/JB095iB10p15695

Zhang, Y. (1999). A criterion for the fragmentation of bubbly magma based on brittle failure theory. *Nature* 402, 648–650. doi: 10.1038/45210

Zobin, V. M., Luhr, J. F., Taran, Y. A., Breton, M., Cortes, A., De La Cruz-Reyna, S., et al. (2002). Overview of the 1997-2000 activity of Volcan de Clima, Mexico. *J. Volcanol. Geotherm. Res.* 117, 1–19. doi: 10.1016/S0377-0273(02)00232-9